Results in Physics 51 (2023) 106660

Contents lists available at ScienceDirect

Results in Physics

journal homepage: www.elsevier.com/locate/rinp

Broadband long-wave infrared metamaterial absorbers based on germanium resonators

Fuming Yang [a,b,c], Zhongzhu Liang [a,b,c,*], Xiaoyan Shi [a], Xiqing Zhang [a], Dejia Meng [b], Rui Dai [a], Shoutao Zhang [a], Yan Jia [a], Ningte Yan [a], Sixuan Li [a], Zihan Wang [a]

[a] *Center for Advanced Optoelectronic Functional Materials Research and Key Laboratory of UV Light-Emitting Materials and Technology of Ministry of Education, College of Physics, Northeast Normal University, Changchun 130024, China*

[b] *Changchun Institute of Optics, Fine Mechanics and Physics, Chinese Academy of Sciences, Changchun, Jilin 130033, China*

[c] *University of the Chinese Academy of Sciences, China*

A B S T R A C T

The broadband metamaterial perfect absorbers over various incident angles are highly significant in long-wave infrared (LWIR) detection. Previous research on LWIR metamaterial absorbers has mainly focused on metallic resonators. Here, we propose two broadband LWIR metamaterial absorbers that use dielectric resonators instead. The germanium (Ge) resonators on the top layer excite resonance modes that control the equivalent impedance of the structure, which acts on the high-lossy Si_3N_4-Ti reflecting layer to assume the absorption. Firstly, we designed a three-layer structure of Ge-Si_3N_4-Ti, which achieved a broadband absorption with an average absorptivity of 93.1 % in the 8–12 μm range. The absorption ratio of metal can be effectively reduced by replacing the metal. Then, to further enhance the absorptivity, we inserted a Si_3N_4 layer into the Ge layer, increasing the 90 % absorption bandwidth to 7.96–14.16 μm and the average absorptivity in 8–14 μm to 96.5 %. Compared to metamaterial absorbers based on metallic resonators, dielectric resonators with a large feature size make fabricating easier. Our proposed metamaterial absorber provides ultra-wideband absorption covering the LWIR range. In addition, it is insensitive to the incident angle, making it a potential candidate for thermal imaging and broadband thermal emission applications.

Introduction

Efficient detection of electromagnetic wave signals requires devices with good absorption capabilities. In the long-wave infrared band (8–14 μm), broadband absorbers are crucial for applications such as thermal imaging [1,2], radiation cooling [3], and thermal emission [4–6]. However, it isn't easy to meet the needs of broadband absorption due to the limitations of the material band gap. Increasing the film thickness to enhance absorption will increase the heat capacity of the system, thereby reducing the sensitivity of the detection. The emergence of metamaterial absorbers provides a new way of designing broadband absorbers with thin structures. Since the perfect metamaterial absorber was proposed by Landy et al. in 2008 [7], research on metamaterial absorbers has expanded to cover a wide range of regions from visible light to microwaves [8–14] according to their excellent performance.

Broadband absorption in metamaterial absorbers requires the combined action of multiple relatively independent absorption modes with similar frequency differences, as the bandwidth provided by a single enhanced absorption mode alone is not enough [15]. The position of the absorption peak in the metamaterial is related to the size of the resonators. Therefore, among the reported methods, the most commonly used is to stack several resonators of different wavelengths horizontally [16,17] or vertically [18]. For example, Ding et al. used the metal-dielectric multilayered quadrangular frustum pyramids to lead the broadband absorption in the microwave band [19]. And Kim et al. achieved a similar broadband absorption effect through a truncated cone structure [20]. However, the vertically stacked metamaterials with increased structural layers are difficult to manufacture, especially for higher frequency absorbers. Guo et al. propose a broadband metamaterial absorber based on multiple horizontal structures, and the simulated total absorption exceed 90% from 7.8 to 12.1 um [18]. Still, the overall absorption efficiency of the horizontally stacked metamaterial absorber will be disturbed by the coupling effect between resonators. Another way is to introduce high-loss materials into the structure to expand the resonance peak's absorption bandwidth [21], such as Ti [22,23], Cr [24,25], W [26,27], and other high-loss metals. For instance, Ran et al. used a four-layer nitride absorber that provides perfect absorption within 260–1510 nm [28]. In the LWIR band, lossy dielectric materials such as SiN [29,30] and SiO_2 [22,31] can also enhance absorptivity. Still, their absorption capacity is limited by the

* Corresponding author.
E-mail address: liangzz@nenu.edu.cn (Z. Liang).

https://doi.org/10.1016/j.rinp.2023.106660
Received 15 February 2023; Received in revised form 15 June 2023; Accepted 17 June 2023
Available online 22 June 2023

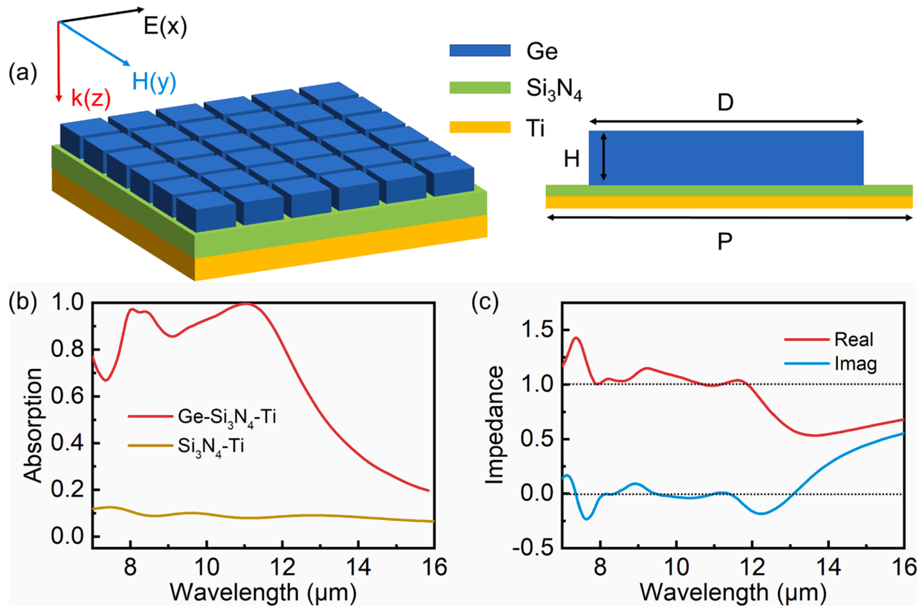

Fig. 1. (a) Structure diagram of the Ge-Si_3N_4-Ti broadband absorber. The period of the unit cell *P* is 5.8 μm. The side length of the Ge resonator *D* is 4.8 μm, and the height *H* is 0.6 μm. The Si_3N_4 and Ti layer thickness are 0.1 μm and 0.15 μm. (b) Absorption curves of Ge-Si_3N_4-Ti absorbers and Si_3N_4-Ti layer only. (c) The equivalent impedance of metamaterial absorbers.

dielectric layer's material loss coefficient and thickness, which requires a larger thickness to achieve a higher absorptivity. However, for Metal-Dielectric-Metal (MDM) structured metamaterial absorbers, increasing the thickness of the dielectric layer will affect the resonance between the upper and lower metals, thereby losing the absorption efficiency.

Here, we propose a design method for ultra-wideband LWIR metamaterial absorbers based on Ge dielectric resonators instead of metallic resonators in classic metamaterial absorbers. Firstly, we designed a Ge-Si_3N_4-Ti broadband metamaterial absorber. In the absence of Ge resonators, the high-loss Ti layer and the Si_3N_4 layer act as a reflection layer. And under the control of the Ge resonators, it can excite several efficient absorption modes, achieving perfect absorption at 8.03 μm and 11.03 μm, with an average absorptivity of 93.1 % in the 8–12 μm range. On this basis, we further improved the absorption efficiency of the absorber by inserting a Si_3N_4 layer into the middle of the Ge resonator, resulting in improved absorption intensity and expanded absorption bandwidth of 96.5 % within the 8–14 μm range. The above results achieve ultra-wide absorption covering the LWIR band, showing polarization-insensitive and incident-angle-insensitive properties. Therefore, the proposed metamaterial absorbers can play a potential role in thermal imaging, broadband thermal emission, and other fields.

Ge-Si_3N_4-Ti broadband absorber

The structure of the proposed Ge-Si_3N_4-Ti broadband absorbers is shown in Fig. 1 (a), which consists of periodic Ge nano-cubes on Si_3N_4-Ti films with a period cell of 5.8 μm. The thicknesses of the Ge, Si_3N_4, and Ti layers are 0.6 μm, 0.1 μm, and 0.15 μm, respectively. The finite difference time domain method was used to simulate the absorber's performance, with the optical parameters of Ge, Si_3N_4, and Ti materials obtained from Palik [32], Kischkat [33], and Rakic [34], respectively. Both Si_3N_4 and Ti materials have the ability to absorb long-wave infrared light, and Ge nano-cubes act as resonators to control the light response characteristics of the structure. Since the absorber form is polarization-independent, linearly polarized light is used along the X-axis direction in the electric field direction for simulation. The absorption curve of the Ge-Si_3N_4-Ti absorber is shown in Fig. 1(b). The absorptivity (*A*) is determined by: $A = 1 - R - T$, *R* and *T* are the reflectivity and transmittance, respectively. Since the thickness of the metal covering the bottom is large enough to exceed the skin depth of Ti in the LWIR band, the light cannot penetrate, and the absorptivity can be corrected to $A = 1 - R$. In the absence of the top-layer Ge resonators, the absorptivity of the underlying Si_3N_4-Ti film remains at about 10 %, as depicted by the yellow line in Fig. 1 (b), which means most of the energy is being reflected back, as if there were a high-reflection layer with a barrier. At this time, the absorption intensity is weak. Next, by placing lossless Ge resonators above the Si_3N_4-Ti film, it is possible to achieve a broadband absorption effect in the LWIR band. Through the geometric size design of Ge nano-cubes, we realized a high absorptivity of 97.6 % and 99.6 % at the absorption peaks of 8.03 μm and 11.03 μm, respectively, as shown in the red line in Fig. 1 (b). The average absorptivity in the 8–12 μm range is 93.1 %. Matching the metamaterial absorber's structural impedance with the external environmental impedance eliminates the reflection resulting in perfect absorption. The equivalent impedance of the metamaterial absorber can be calculated by extracting the structural S parameters, which can be expressed as [35]:

$$Z = \sqrt{\frac{(1+S_{11})^2 - S_{21}^2}{(1-S_{11})^2 - S_{21}^2}} \tag{1}$$

where $Z = Z' + iZ''$, Z' and Z'' are the real and imaginary parts of the equivalent impedance. When the impedance of the absorber is equal to the environmental impedance ($Z_{air} = 1$), the impedance matching is achieved to reach perfect absorption. According to $R = \frac{(Z'-1)^2+(Z'')^2}{(Z'+1)^2+(Z'')^2}$ [36], the reflectivity depends on the degree of adaptation of the effective impedance to the air, so the key to broadband absorption is maintaining the impedance-matching condition over a wide range. As shown in Fig. 1 (c), the absorber's impedance at two absorption peaks of 8.03 μm and 11.03 μm is $Z_{8.03} = 1.021$——0.022i and $Z_{11.03} = 0.991 + 0.002i$, which is close to the perfect absorption condition. Fig. 1 (c) describes the relationship between the real and imaginary parts of the equivalent impedance of the absorber and the wavelength. In the range of 8–12 μm, the real part of *Z* is close to 1, and the imaginary part is close to 0. This result indicates that the structure achieves or approaches impedance matching in the broadband range under the coupling effect of different resonances excited by the Ge resonator, which is consistent with the absorption curve.

We analyzed the absorption effect of each absorption layer and

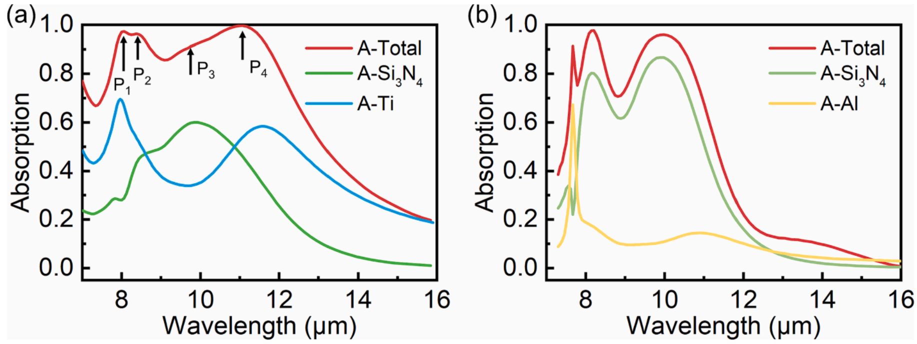

Fig. 2. (a) Absorption contribution of different absorption layers. (b) Absorption contribution of different absorption layers when the bottom metal is Al.

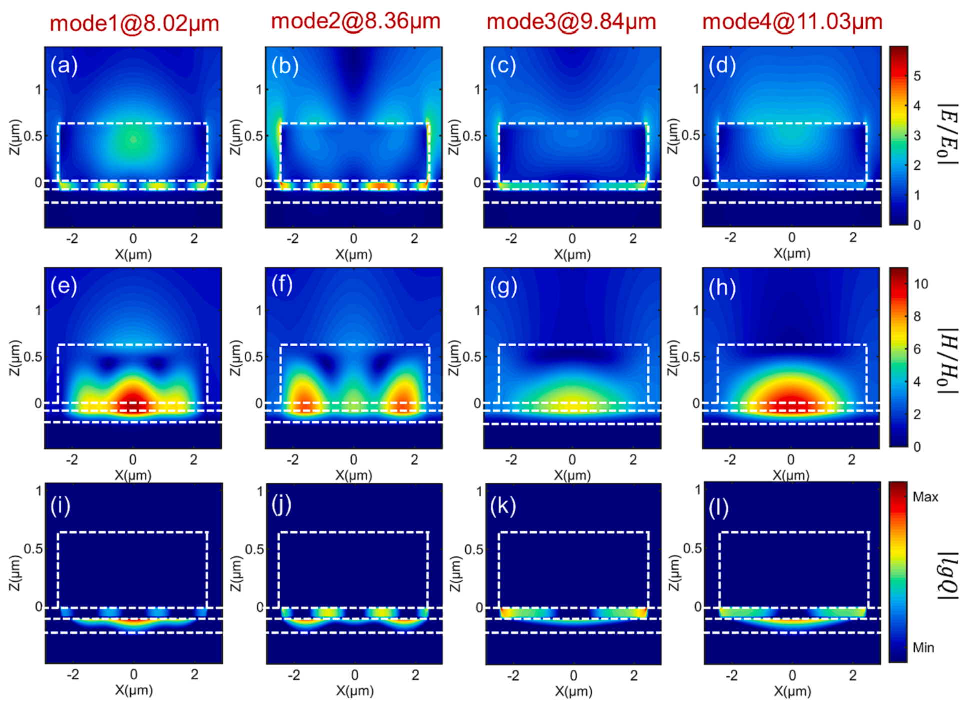

Fig. 3. Local electromagnetic field and energy distribution of mode1-mode4: (a) - (d) Electric field distribution; (e) - (h) Magnetic field distribution; (i) - (l) Energy distribution.

observed the energy loss between different material layers in Fig. 2 (a). It was evident that the Ge layer has weak absorption capabilities, and the underlying Si_3N_4-Ti layer absorbs most of the energy. At 8–12 μm, the highly lossy metal Ti has a high absorption intensity, especially at P_1 (8.03 μm) and P_4 (11.03 μm), which matches the absorber's absorption peak position. For the Si_3N_4 layer, the absorptivity at P_2 (8.36 μm) is significantly improved, and the absorption peak is reached at P_3 (9.84 μm). The difference in absorption efficiency between the absorption layers corresponds to the difference in response of different resonance modes. However, in some applications of optoelectronic devices, metal absorption inhibits the generation of photoelectrons, and the accompanying heat lossy effect is also undesirable. Therefore, it is important to avoid metal absorption as much as possible.

The absorption of the metal in the classical MDM absorbers is difficult to avoid as the metal resonators participate in the excitation resonance. However, the absorption only occurs in the bottom Si_3N_4-Ti loss layer in our absorbers, which helps prevent the ohmic absorption of the metal, allowing for low ohmic loss broadband absorption. For this reason, we replaced the metal layer with a high-reflectivity metal Al, and the obtained absorption curves are shown in Fig. 2 (b). Overall, the reflective layer composed of Si_3N_4-Al maintains its function, ensuring broadband absorption in 8–12 μm, although the absorption bandwidth decreases. At the same time, most of the energy is absorbed by the Si_3N_4 layer, and the absorptivity of the underlying metal falls from 57.6 % to 16.5 %, effectively avoiding metallic absorption. In addition, the sharp metal absorption enhancement effect at 7.7 μm is caused by high-order resonance, which can also be suppressed by changing the geometric parameters of the resonator. Compared with the MDM metamaterial absorbers, we achieve impedance matching and broadband absorption by adjusting the geometric parameters of the dielectric resonator, thus effectively avoiding the lossy impact of the top metal resonator. Only the lower lossy material layer bears the absorption effect. When the high-reflectivity metal is used as the reflective substrate, the lossy effect of the underlying metal can also be effectively reduced so that the absorption of the dielectric material is dominant, which is helpful for the effective excitation of photoelectrons. This design method can provide a reference for metamaterial absorbers used in optoelectronic devices.

We analyzed four different absorption modes (mode1 at 8.03 μm, mode2 at 8.36 μm, mode3 at 9.84 μm, and mode4 at 11.03 μm) and extracted their near-field electromagnetic field and energy distribution as depicted in Fig. 3. As shown in Fig. 3 (a) and (e), Mode1 exhibited electrical resonance, with the electric field concentrated in the Ge

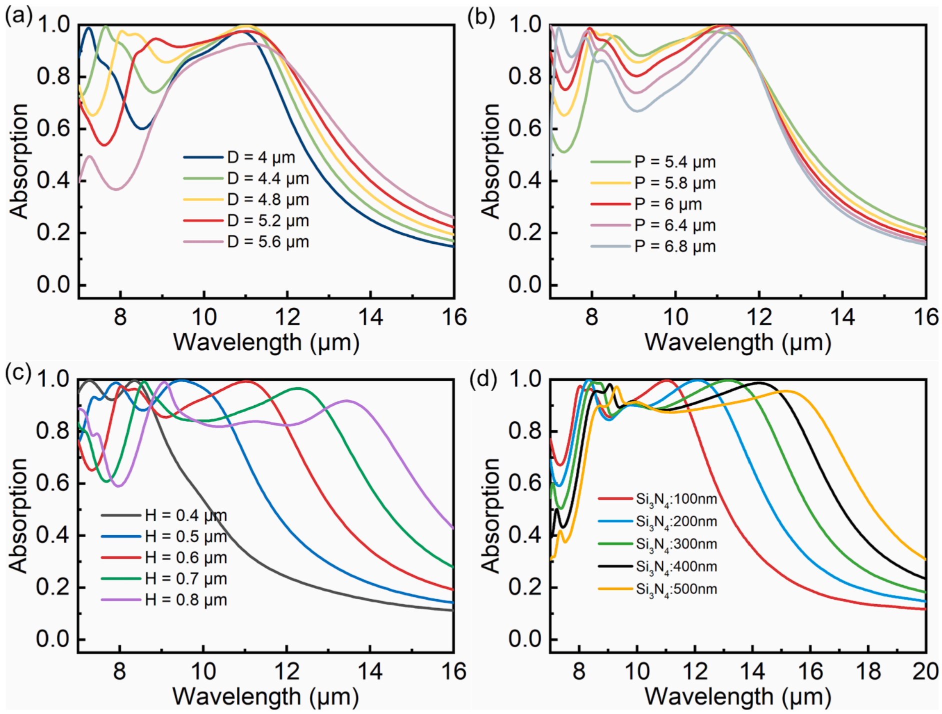

Fig. 4. Effect of structural parameters of Ge resonator on absorptivity: (a) Length; (b) Period; (c) Height; (d) Thickness of Si_3N_4.

resonator along the X direction and the magnetic field distributed below the junction of the resonator and the Si_3N_4-Ti lossy layer along the Y direction. As shown in Fig. 3 (b) and (f), Mode2 showed a second-order magnetic dipole mode, with two co-directional electric circulations in the Si3N4 layer exciting two positive magnetic currents along the Y-axis. As shown in Fig. 3 (c) and (g), Mode3 had the electromagnetic field concentrated in the Si3N4 layer below the edge of the Ge resonator, with the electric field directions on both sides of the resonator being positive and negative along the Z-axis, respectively. The reverse circulation excited the positive magnetic current along the Y-axis, consistent with the characteristics of the magnetic dipole mode. As shown in Fig. 3 (d), (h), mode4 with lower frequency is an F-P-like mode. The electric field is distributed within the resonator, parallel to the direction of the incident electric field. Conversely, the magnetic field is concentrated on the interface between the Ge resonator and the lossy layer. If the resonant wavelength of mode4 satisfies the destructive interference condition, the reflectivity reaches 0, namely:

$$\frac{2\pi}{\lambda} n \bullet 2L = (2k+1)\pi \tag{2}$$

Where n is the refractive index of the medium in the resonant cavity, L is the cavity length, k is the order of the F-P mode, and λ is the wavelength. The wavelength of the first-order F-P mode calculated according to equation (2) is 10.75 μm, which is in agreement with the position of the absorption peak mode4. The energy lossy of light in the lossy material depends on the intensity of the excitation electric field and the loss coefficient of the material, that is [36]:

$$Q(\omega) = 0.5 \times \omega \times \varepsilon'' \times |E(\omega)|^2 \tag{3}$$

Where ω is the frequency of light, ε“ is the imaginary part of the dielectric constant, and E is the electric field strength. Fig. 3 (i) - (l) showcases the lossy contribution distribution of the absorber calculated according to equation (3). For a clear image, Q applied the logarithm. The results indicate no energy loss in the Ge resonator, whereas the Si_3N_4 and Ti layers experience energy loss. Depending on the mode, the lossy area is either concentrated in the Ti layer below the Si_3N_4 layer or the Si_3N_4 layer. This means that the absorption of Ti dominates for mode1 and mode4, while Si_3N_4 dominates for mode2 and mode3. The Z-direction electric field generated by these two modes corresponds to the transverse propagation mode perpendicular to the Z-axis. This field

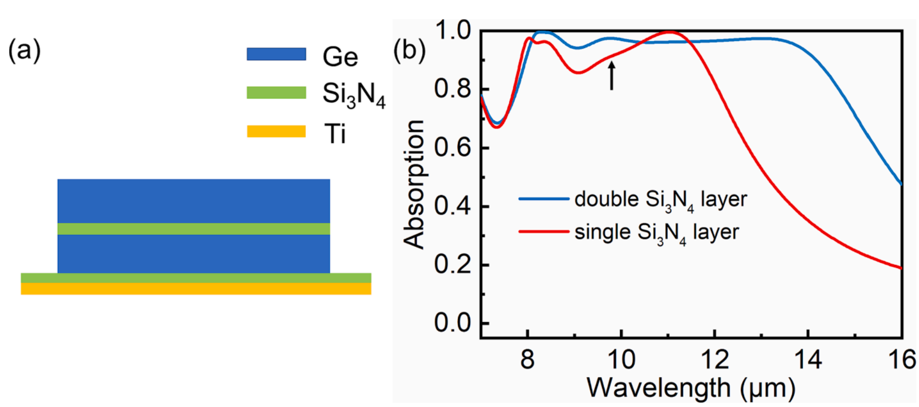

Fig. 5. (a) Structure diagram of the double-layer Si_3N_4 ultra-wideband absorber. (b) Absorption curves of the absorbers.

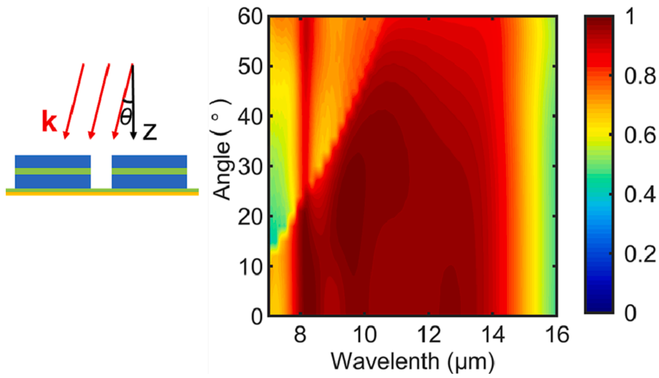

Fig. 6. The performance of the absorber in different incident angles.

effectively captures the electromagnetic wave in the lossy material, increasing the effective propagation distance of light in Si_3N_4, thereby improving the absorptivity.

The absorber's absorption curve is affected by the size and gap of the Ge resonators, including the position and coupling strength of each resonance. As shown in Fig. 4, we simulate the changes in absorption spectra under different geometric parameters. As shown in Fig. 4 (a), mode1 and mode2 are sensitive to the size change of the resonator, and their absorption wavelengths increase with the increase of the resonator's diameter D. The absorption intensity of the transverse mode3 decreases with the increase of the resonator spacing, as shown in Fig. 4 (b). In addition, the response of the absorber is sensitive to the thickness of the Ge resonator. When the height H of the resonator increases, all absorption peaks have different degrees of redshift, as shown in Fig. 4 (c). The F-P-like mode is sensitive to the thickness of the structure. Therefore, when the size and spacing of the resonator change, the absorptivity and absorption wavelength of mode4 do not change significantly. Similarly, the thickness of the Si_3N_4 lossy layer also changes the absorption wavelength of mode4, as shown in Fig. 4 (d), while its effect on other absorption peaks is not prominent. Therefore, increasing the thickness of the Si_3N_4 can expand the absorption bandwidth, although this will decrease the average absorptivity.

Double-layer Si_3N_4 ultra-wideband absorber

In the previously designed broadband absorber, the absorptivity near 9 μm decreases significantly, as shown in the red line in Fig. 5 (b), which affects the overall absorption efficiency of the structure. Moreover, this decrease will not be improved by increasing the thickness of the Si_3N_4 lossy layer, as shown in Fig. 4 (d). Therefore, we broaden the absorption spectrum by inserting a Si_3N_4 absorption layer into the Ge resonator. The structure of the proposed double-layer Si_3N_4 ultra-wideband absorber is shown in Fig. 5 (a). In order to improve the lossy of Si_3N_4 layer to increase the absorption intensity, we inserted a 200 nm thick Si_3N_4 layer in the middle of the Ge resonator, and the remaining parameters were consistent with the previous ones. The absorption curve of the ultra-wideband absorber obtained is shown in the blue line in Fig. 5 (b). Compared with the previous results, the absorptivity and absorption bandwidth has been significantly improved. The 90 % absorption bandwidth is 7.96 μm to 14.16 μm, totaling 6.2 μm, and the average absorptivity in the range of 8–14 μm is 96.5 %. The newly introduced Si_3N_4 interlayer has two effects on improving the absorber's performance. Firstly, for the F-P-like resonant mode4, the Si_3N_4 interlayer increases the equivalent thickness of the resonant cavity and redshifts the resonant wavelength, which improves the absorption range. Secondly, unlike the case where only the thickness of the lower Si_3N_4 is increased, the absorptivity of the transverse mode3 is significantly improved, which avoids the decrease in the absorption intensity caused by the separation of the resonance peaks. The performance of the double-layer structure at different incident angles is also simulated, as shown in Fig. 6. θ is the angle with the z-axis of the light propagation direction. The absorption capacity of the absorber has not been significantly degraded at an incident angle of 60°, indicating that it is has good incident angle insensitivity.

In Table 1, we have compared the performance of the proposed LWIR broadband absorbers with other recently reported absorbers. Compared with absorbers based on metallic nanoarrays, the proposed absorbers based on Ge resonators have a simpler configuration and larger structure size, giving them an advantage in the preparation. Additionally, our absorption efficiency is higher, and the device's thickness is smaller than the all-dielectric absorption mentioned in Ref. [39].

Conclusion

In summary, we propose two broadband metamaterial absorbers in the LWIR band based on Ge resonators, and the average absorptivity of the $Ge-Si_3N_4-Ti$ absorber in 8–12 μm range is 93.1 %. Then, the absorption intensity of the absorber is significantly improved by inserting Si_3N_4 in the middle of the resonator, which expands the absorption range. The average absorptivity of the double-layer Si_3N_4 ultra-wideband absorber in 8–14 μm is 96.5 %. The transverse size of the designed absorber is about 1/2 central wavelength, and the longitudinal size is 1/12 of the central wavelength. The tiny device's thickness makes it light and thin, which is crucial in optoelectronic devices. At the same time, the larger lateral size provides a wealth of lateral modes and reduces the difficulty of preparing microstructures. By controlling the reflective metal at the bottom of the resonant mode, the energy can be concentrated in the lossy dielectric layer, which helps to improve the detector's efficiency. We believe that the broadband absorbers can play a potential role in thermal imaging, thermal emission, radiation regulation, and other fields.

Funding. National Natural Science Foundation of China (61735018); The Science Fund for Distinguished Young Scholars of Jilin Province(20230201080GX); Scientific and Technological Development Project of Jilin Province (20220201080GX); Excellent Member of Youth Innovation Promotion Association of the Chinese Academy of Sciences (Y201836); Leading Talents and Team Project of Scientific and Technological Innovation for Young and Middle-aged Groups in Jilin Province (20190101012JH).

CRediT authorship contribution statement

Fuming Yang: Conceptualization, Methodology, Software, Formal

Table 1
Comparison of representative structure of LWIR broadband absorbers in recent years.

Work by	Nanoarray Configuration	Material layer distribution	Average absorptivity	Range bandwidth	Period
[37]	nano cross surrounding	$Cr-Ge-Si_3N_4-Ti$	94.1%	8.98–16.21 μm	3.1 μm
[38]	Cross	Ti-Si-Al	94%	7.5–13.25 μm	1.6 μm
[39]	Square	$Si-Si_3N_4$	90.36%	8–14 μm	6 μm
[40]	Central ring with four semi-elliptical rings	$Ti-Ge-TiO_2-Ti$	99.7%	9.7–12 μm	2 μm
[41]	Graphene-Metal fractal cross	Metal-Graphene-Dielectric-Metal	92.1%	8–12 μm	5 μm
This work	SquareSquare	$Ge-Si_3N_4-Ti$	93.1%96.5%	8–12 μm	5.8 μm
		$Ge-Si_3N_4-Ge-Si_3N_4Ti$		8–14 μm	5.8 μm

analysis, Writing – original draft. **Zhongzhu Liang:** Resources, Writing – review & editing, Supervision, Funding acquisition. **Xiaoyan Shi:** Investigation. **Xiqing Zhang:** Data curation. **Dejia Meng:** Project administration, Methodology. **Rui Dai:** . **Shoutao Zhang:** . **Yan Jia:** . **Ningte Yan:** Visualization. **Sixuan Li:** . **Zihan Wang:** Software.

Declaration of Competing Interest

The authors declare that they have no known competing financial interests or personal relationships that could have appeared to influence the work reported in this paper.

Data availability

Data will be made available on request.

References

[1] Du K, Li Q, Zhang W, Yang Y, Qiu M. Wavelength and Thermal Distribution Selectable Microbolometers Based on Metamaterial Absorbers. IEEE Photonics J 2015;7(3). 1–8.https://ieeexplore.ieee.org/abstract/document/7047761/.
[2] Ma W, Jia D, Wen Y, Yu X, Feng Y, Zhao Y. Diode-based microbolometer with performance enhanced by broadband metamaterial absorber. Opt Lett 2016;41 (13):2974–7. https://opg.optica.org/ol/abstract.cfm?URI=ol-41-13-2974.
[3] Li W, Fan S. Nanophotonic control of thermal radiation for energy applications [Invited]. Opt Express 2018;26(12). 15995–16021.https://opg.optica.org/oe/abstract.cfm?URI=oe-26-12-15995.
[4] Barho FB, Gonzalez-Posada F, Cerutti L, Taliercio T. Heavily Doped Semiconductor Metamaterials for Mid-Infrared Multispectral Perfect Absorption and Thermal Emission. Adv Opt Mater 2020;8(6):1901502. https://doi.org/10.1002/adom.201901502.
[5] Dyachenko PN, Molesky S, Petrov AY, Störmer M, Krekeler T, Lang S, et al. Controlling thermal emission with refractory epsilon-near-zero metamaterials via topological transitions. Nat Commun 2016;7(1):11809. https://doi.org/10.1038/ncomms11809.
[6] Qu Y, Li Q, Du K, Cai L, Lu J, Qiu M. Dynamic Thermal Emission Control Based on Ultrathin Plasmonic Metamaterials Including Phase-Changing Material GST. Laser Photonics Rev 2017;11(5):1700091. https://doi.org/10.1002/lpor.201700091.
[7] Landy NI, Sajuyigbe S, Mock JJ, Smith DR, Padilla WJ. Perfect Metamaterial Absorber. Phys Rev Lett 2008;100(20):207402. https://doi.org/10.1103/PhysRevLett.100.207402.
[8] Bilal RMH, Zakir S, Naveed MA, Zubair M, Mehmood MQ, Massoud Y. Nanoengineered nickel-based ultrathin metamaterial absorber for the visible and short-infrared spectrum. Opt Mater Express 2023;13(1). 28–40.https://opg.optica.org/ome/abstract.cfm?URI=ome-13-1-28.
[9] Li Z, Sun X, Ma C, Li J, Li X, Guan B-O, et al. Ultra-narrow-band metamaterial perfect absorber based on surface lattice resonance in a WS2 nanodisk array. Opt Express 2021;29(17):27084–91. https://opg.optica.org/oe/abstract.cfm?URI=oe-29-17-27084.
[10] Chang Q, Liu Z, Liu Z, Fu G, Liu X, Liu G. Silicon-based asymmetric dimer-resonator grating for narrowband perfect absorption and sensing. Opt Express 2023;31(3). 4190–4198.https://opg.optica.org/oe/abstract.cfm?URI=oe-31-3-4190.
[11] Qin Z, Shi X, Yang F, Hou E, Meng D, Sun C, et al. Multi-mode plasmonic resonance broadband LWIR metamaterial absorber based on lossy metal ring. Opt Express 2022;30(1). 473–483.https://opg.optica.org/oe/abstract.cfm?URI=oe-30-1-473.
[12] Zhuang X, Zhang W, Wang K, Gu Y, An Y, Zhang X, et al. Active terahertz beam steering based on mechanical deformation of liquid crystal elastomer metasurface. Light Sci Appl 2023;12(1):14. https://doi.org/10.1038/s41377-022-01046-6.
[13] Zhang C, Yin S, Long C, Dong BW, He D, Cheng Q. Hybrid metamaterial absorber for ultra-low and dual-broadband absorption. Opt Express 2021;29(9). 14078–14086.https://opg.optica.org/oe/abstract.cfm?URI=oe-29-9-14078.
[14] J. Ning, S. Dong, X. Luo, K. Chen, J. Zhao, T. Jiang, and Y. Feng, "Ultra-broadband microwave absorption by ultra-thin metamaterial with stepped structure induced multi-resonances," Results in Physics **18** (2020) 103320.https://www.sciencedirect.com/science/article/pii/S2211379720317873.
[15] Wang B-X, Xu C, Duan G, Xu W, Pi F. Review of Broadband Metamaterial Absorbers: From Principles, Design Strategies, and Tunable Properties to Functional Applications. Adv Funct Mater 2023;n/a(n/a):2213818. https://doi.org/10.1002/adfm.202213818.
[16] Cui Y, Fung KH, Xu J, Ma H, Jin Y, He S, et al. Ultrabroadband Light Absorption by a Sawtooth Anisotropic Metamaterial Slab. Nano Lett 2012;12(3):1443–7. https://doi.org/10.1021/nl204118h.
[17] Du C, Zhou D, Guo H-H, Pang Y-Q, Shi H-Y, Liu W-F, et al. An ultra-broadband terahertz metamaterial coherent absorber using multilayer electric ring resonator structures based on anti-reflection coating. Nanoscale 2020;12(17):9769–75. https://doi.org/10.1039/C9NR10668E.
[18] Guo W, Liu Y, Han T. Ultra-broadband infrared metasurface absorber. Opt Express 2016;24(18). 20586–20592.https://opg.optica.org/oe/abstract.cfm?URI=oe-24-18-20586.
[19] Ding F, Cui Y, Ge X, Jin Y, He S. Ultra-broadband microwave metamaterial absorber. Appl Phys Lett 2012;100(10):103506. https://doi.org/10.1063/1.3692178.
[20] Kim YJ, Yoo YJ, Kim KW, Rhee JY, Kim YH, Lee Y. Dual broadband metamaterial absorber. Opt Express 2015;23(4). 3861–3868.https://opg.optica.org/oe/abstract.cfm?URI=oe-23-4-3861.
[21] R. Khosravi, Y. E. Monfared, and M. Qasymeh, "Ultra-broadband nearly perfect absorbers based on graphene-coated lossy metallic nanostructures," Results in Physics **36** (2022) 105470.https://www.sciencedirect.com/science/article/pii/S2211379722002212.
[22] Zhou Y, Qin Z, Liang Z, Meng D, Xu H, Smith DR, et al. Ultra-broadband metamaterial absorbers from long to very long infrared regime. Light Sci Appl 2021;10(1):1–12. https://doi.org/10.1038/s41377-021-00577-8.
[23] Yu P, Yang H, Chen X, Yi Z, Yao W, Chen J, et al. "Ultra-wideband solar absorber based on refractory titanium metal," Renew. Energy 2020;158. 227–235.https://www.sciencedirect.com/science/article/pii/S0960148120308478.
[24] Qian Q, Sun T, Yan Y, Wang C. Large-Area Wide-Incident-Angle Metasurface Perfect Absorber in Total Visible Band Based on Coupled Mie Resonances. Adv Opt Mater 2017;5(13):1700064. https://doi.org/10.1002/adom.201700064.
[25] Liang Y, Liu X, Xin J, Zhang X, Wang Y, Song Y. Ultra-broadband long-wave infrared metasurface absorber based on Peano fractal curve. Results Phys 2022;33:105169. https://www.sciencedirect.com/science/article/pii/S2211379721011244.
[26] Jiang X, Wang T, Zhong Q, Yan R, Huang X. Ultrabroadband light absorption based on photonic topological transitions in hyperbolic metamaterials. Opt Express 2020;28(1). 705–714.https://opg.optica.org/oe/abstract.cfm?URI=oe-28-1-705.
[27] S. Mahmud, S. S. Islam, K. Mat, M. E. H. Chowdhury, H. Rmili, and M. T. Islam, "Design and parametric analysis of a wide-angle polarization-insensitive metamaterial absorber with a star shape resonator for optical wavelength applications," Results in Physics **18** (2020) 103259.https://www.sciencedirect.com/science/article/pii/S2211379720317265.
[28] Y. Ran, Z. Jiang, and Z. Wang, "All-nitride broadband metamaterial absorbers," Results in Physics **38** (2022) 105657.https://www.sciencedirect.com/science/article/pii/S2211379722003552.
[29] Chen C, Huang Y, Wu K, Bifano TG, Anderson SW, Zhao X, et al. Polarization insensitive, metamaterial absorber-enhanced long-wave infrared detector. Opt Express 2020;28(20). 28843–28857.https://opg.optica.org/oe/abstract.cfm?URI=oe-28-20-28843.
[30] Üstün K, Turhan-Sayan G. Wideband long wave infrared metamaterial absorbers based on silicon nitride. J Appl Phys 2016;120(20):203101. https://doi.org/10.1063/1.4968014.
[31] Raman AP, Anoma MA, Zhu L, Rephaeli E, Fan S. Passive radiative cooling below ambient air temperature under direct sunlight. Nature 2014;515(7528):540–4. https://doi.org/10.1038/nature13883.
[32] Palik ED. Handbook of optical constants of solids. (Academic press; 1998.
[33] Kischkat J, Peters S, Gruska B, Semtsiv M, Chashnikova M, Klinkmüller M, et al. Mid-infrared optical properties of thin films of aluminum oxide, titanium dioxide, silicon dioxide, aluminum nitride, and silicon nitride. Appl Opt 2012;51(28). 6789–6798.https://opg.optica.org/abstract.cfm?uri=ao-51-28-6789.
[34] Rakić AD, Djurišić AB, Elazar JM, Majewski MLJAO. Optical properties of metallic films for vertical-cavity optoelectronic devices. Appl Opt 1998;37(22). 5271–5283.https://opg.optica.org/abstract.cfm?uri=ao-37-22-5271.
[35] Smith D, Vier D, Koschny T, Soukoulis CJPRE. Electromagnetic parameter retrieval from inhomogeneous metamaterials. Phys Rev E 2005;71(3):036617. https://doi.org/10.1103/PhysRevE.71.036617.
[36] Tittl A, Harats MG, Walter R, Yin X, Schäferling M, Liu N, et al. Quantitative Angle-Resolved Small-Spot Reflectance Measurements on Plasmonic Perfect Absorbers: Impedance Matching and Disorder Effects. ACS Nano 2014;8(10):10885–92. https://doi.org/10.1021/nn504708t.
[37] S. Liang, F. Xu, H. Yang, S. Cheng, W. Yang, Z. Yi, Q. Song, P. Wu, J. Chen, and C. Tang, "Ultra long infrared metamaterial absorber with high absorption and broad band based on nano cross surrounding," Optics & Laser Technology **158** (2023) 108789.https://www.sciencedirect.com/science/article/pii/S0030399222009355.
[38] Qin Z, Meng D, Yang F, Shi X, Liang Z, Xu H, et al. Broadband long-wave infrared metamaterial absorber based on single-sized cut-wire resonators. Opt Express 2021;29(13). 20275–20285.https://opg.optica.org/oe/abstract.cfm?URI=oe-29-13-20275.
[39] Chen C, Liu Y, Jiang Z-Y, Shen C, Zhang Y, Zhong F, et al. Large-area long-wave infrared broadband all-dielectric metasurface absorber based on maskless laser direct writing lithography. Opt Express 2022;30(8). 13391–13403.https://opg.optica.org/oe/abstract.cfm?URI=oe-30-8-13391.
[40] L. Sun, D. Liu, J. Su, X. Li, S. Zhou, K. Wang, and Q. Zhang, "Near Perfect Absorber for Long-Wave Infrared Based on Localized Surface Plasmon Resonance," Nanomaterials (2022).https://www.mdpi.com/1971754.
[41] T. Xie, D. Chen, Y. Xu, Y. Wang, M. Li, Z. Zhang, and J. Yang, "High absorption and a tunable broadband absorption based on the fractal Technology of Infrared Metamaterial Broadband Absorber," Diamond and Related Materials **123** (2022) 108872.https://www.sciencedirect.com/science/article/pii/S0925963522000541.